SAND2020-6337J

Influence of ozone addition on the low-temperature oxidation of dimethyl ether in a jet-stirred reactor

Handong Liao[a], Shiqing Kang[a], Nils Hansen[b], Feng Zhang[c], Bin Yang[a,*]

[a]*Center for Combustion Energy and Key Laboratory for Thermal Science and Power Engineering of MOE, Tsinghua University, Beijing 100084, PR China*

[b]*Combustion Research Facility, Sandia National Laboratories, Livermore, CA 94551, USA*

[c]*National Synchrotron Radiation Laboratory, University of Science and Technology of China, Hefei, Anhui, 230026, P. R. China*

Abstract: The influence of ozone addition on the low-temperature oxidation of dimethyl ether (DME) was investigated experimentally in an atmospheric-pressure jet-stirred reactor, over the temperature range of 400-800 K. By employing the synchrotron vacuum ultraviolet photoionization mass spectrometry, detailed speciation information was obtained. Experimental results reveal that the ozone addition has a positive influence on the production of the highly reactive intermediates. Moreover, the low-temperature reactivity of DME was significantly enhanced, which resulted in the broadening of the temperature window of fuel consumption and intermediates formation at lower temperatures. Therefore, novel experimental data from a low temperature regime (400 – 500 K) could be obtained. The data set from this special temperature regime, together with modelling analysis based on two existing DME models (Metcalfe et al. (2013) and Wang et al. (2015)) with an ozone sub-mechanism (Zhao et al. (2016)), yielded insights into the DME low-temperature kinetics. The analysis showed that temperature-sensitive reactions such as the second oxygen channel could be nearly "frozen" at this low temperature (T < 440 K). Furthermore, the production of some intermediates was found to be strongly governed by reaction pairs, such as $CH_3OCH_2 + O_2 = CH_3OCH_2O_2$ and $CH_3OCH_2 + O_2 = 2CH_2O + OH$ for the CH_2O formation. This finding could be useful to examine branching ratios in both models, and the analysis suggested the further modification of the branching ratios for the oxygen addition to $CH_3OCH_2O_2$ pathways and the $CH_3OCH_2O_2$ self-reactions were required. Finally, the influences of the O_3 addition in the sensitive reactions of the fuel initial low-temperature oxidation, are investigated in this work. It is interesting to note that O_3 addition could change the dominating

Corresponding author : Email address : byang@tsinghua.edu.cn

reactions in the fuel low-temperature oxidation, by the addition of some O_3-related pathways with relatively high sensitivity.

Keywords: Ozone assisted low-temperature oxidation, DME, Jet-stirred reactor, Synchrotron vacuum ultraviolet photoionization mass spectrometry, Ozone effect

1. Introduction

To meet stringent emission regulations as well as solve future fossil fuel supply issues, there is a growing need to find alternative feedstock. Dimethyl ether (DME) has been proposed to be a promising alternative fuel. It has also worked as an additive to diesel fuel for its high cetane number (>55) and low NOx and soot emissions [1,2].

Given its great prospect for energy conversion applications, DME oxidation has been extensively studied in past decades, especially for its typical two-stage low temperature oxidation [3-11]. Speciation measurements were first conducted by Dagaut et al. [3] for DME oxidation in a jet-stirred reactor (JSR) at 10 atm, with equivalence ratios varying from 0.2 to 1.0 and temperatures ranging from 550 to 1100 K. The mole fractions of the reactants, stable intermediates and products were quantified with gas chromatography, providing a valuable database for the development of DME oxidation mechanisms. Recently, Moshammer et al. [10,11] provided quantitative information of species related to DME oxidation in the range of 450 − 1000 K. The strong low-temperature and negative temperature coefficient (NTC) behaviors of DME were observed in an atmospheric pressure JSR at a long residence time of 4000 ms and fuel-lean (ϕ = 0.35) conditions. By employing synchrotron vacuum ultraviolet photoionization mass spectrometry (SVUV-PIMS), detection and quantification of the keto-hydroperoxide hydroperoxymethyl formate (HPMF, $HOOCH_2OCHO$) and other oxygenated intermediate species (CH_2O, CH_3OH, H_2O_2, CH_2O_2, CH_3OOH, CH_3OCHO) were achieved. Particularly, the new observation and quantification of HPMF, an indication for the second O_2 addition pathways in the low-temperature oxidation of DME, might impact mechanism development.

To have a better understanding of low-temperature kinetics, the addition of reactive species to promote low-temperature reactivity is a promising experimental method [12-14]. Particularly, ozone, one of such reactive species, has been frequently used as an atomic oxygen carrier [12-14]. Zhao et al. [18] have investigated the low-temperature oxidation of DME, assisted with the seeding of ozone. To this end, the oxidation of DME was studied experimentally at low temperatures (400 - 750 K) in an atmospheric-pressure flow reactor, at residence times from 0.24 to 0.45 s. The addition of ozone, varying from 0 to 1460 ppm, was chosen to investigate the influence of O_3 addition on the DME low-temperature oxidation. The authors found that the presence of O_3 strongly enhances the low-temperature reactivity of DME, and they also observed large discrepancies between model predictions and experimental results. The quantification of a few stable species, using electron-ionization MBMS,

was used to elucidate the observed discrepancies, indicating large uncertainties in some critical reactions of DME low-temperature oxidation. It is worth noting that the flow field of the laminar flow reactor, as well as longitudinal and radial temperature gradients in the reactor, might complicate the sources of uncertainties. Even so, the author showed that the ozone addition could provide some beneficial insights into DME low-temperature kinetics. Some deficiencies of Zhao's experimental approach motivated us to carry out further experimental investigations. We think that work in an ideal reactor using a soft ionization technique followed by mass spectrometry could yield more insights into DME low-temperature oxidation.

In this work, the low-temperature oxidation of DME was investigated in an ideally homogenous jet-stirred reactor [18], with different O_3 addition (1000 ppm and 2000 ppm) and under identical conditions of our previous work [11] to facilitate comparisons. Speciation measurements were performed using SVUV-PIMS and compared with the detailed speciation information of the non-ozone case [10,11]. The goal of this research is 1) to provide detailed speciation information of DME low-temperature oxidation under different ozone addition levels, 2) to explore effects of O_3 addition on the DME low-temperature oxidation kinetics especially at very low temperatures with both experimental and modelling efforts, 3) to offer insights regarding the modelling development under the condition of O_3 addition.

2. Experimental and modeling details

Measurements were carried out at the Chemical Dynamics Beamline of the Advanced Light Source (ALS) at the Lawrence Berkeley National Laboratory (LBNL). The experimental setup and data analysis approaches have been well documented in previous studies [11,20,21]. Briefly, the spherical fused-silica JSR is coupled with a time-of-flight molecular-beam mass spectrometer (TOF-MBMS), using the tunable SVUV radiation as the photoionization (PI) source. The fused silica reactor with a volume of 33.5 cm^3, is located inside an electrically heated chamber. The gaseous compositions are sampled by a quartz nozzle with a ~50μm orifice diameter at the tip. The pressure difference between the reactor (93.3 kPa) and the first pumping stage (~10^{-4} kPa) allows for the formation of a molecular beam, in which the chemical reactions are quenched effectively. The formed molecular beam is skimmed out and after entering a second stage pumping area, the molecular beam is crossed by the synchrotron VUV light. The ionized species are analyzed by a reflectron time-of-flight mass

spectrometer with a mass resolution (m/Δm) of ~4000.

An experimental investigation was performed under steady-state conditions, at 93.3 kPa (700 Torr), with a residence time of τ = 4000 ms. The equivalence ratio ϕ was kept at 0.35 with the initial fuel mole fraction of 2.3%, which was the same as the experimental conditions in Ref. [11,20,21]. The experiments were conducted at two different O_3 seeding concentrations of 1000 ppm and 2000 ppm. Detailed conditions for the investigated conditions are given in Table 1. It is worth mentioning that taking into account the O_2 generation, associated with the O_3 decomposition channel, has practically negligible effect on the value of ϕ (ϕ = 0.348 and 0.346 with 1000 and 2000 ppm O_3 addition, respectively). The gas flows were controlled by calibrated mass flow controllers (MKS), and an ozone generator (Oriel) coupled with a calibrated ozone analyzer was employed to generate and measure the ozone concentration [22]. 15 different temperatures points varying from 400 K to 800 K under two O_3 addition conditions were conducted. The temperature measurements of the reacting mixture were achieved by a thermocouple (K-type, Thermocoax) placed near the sampling position. Good thermal homogeneity along the vertical axis of the reactor has been validated [22]. At each temperature, the experiments were performed at several selected photon energies, to derive species mole fractions. To obtain some insights into ozone-addition effects, a single mass spectra was recorded at a photoionization energy of 11.2eV and the temperature of 540 K for all cases. In addition, measurements of the photoionization efficiency (PIE) spectra were obtained from 9.5 eV to 11.5 eV with 2000 ppm O_3 addition at 540 K for the identification of intermediates .

Table 1 Detailed experimental conditions in the present study.

No.	Equivalence ratio (ϕ)	Pressure	% DME	% O_2	% O_3	% Ar	Residence time	Temperature range
1	0.35	93.3 kPa (700 Torr)	2.30	19.69	0.10	77.91	4000 ms	400 - 800 K
2			2.29	19.67	0.20	77.83		
Ref. [11]			2.30	19.70	0	78.00		460 - 900 K

The mole fractions of species were derived by following the procedure proposed in our recent work [21]. Briefly, the integrated mass signal $S_i(T)$ of a species i can be expressed as a function of its mole fraction x_i as given in Eq. (1) :

$$S_i(T) = C \cdot x_i \cdot \sigma_i(E) \cdot D_i \cdot \varphi(E) \cdot F(k,T,P) \qquad (1)$$

Here, C is a proportionality constant, D_i is the mass discrimination factor, $\sigma_i(E)$ is the photoionization cross section (PICS) of species i at photon energy E, $\varphi(E)$ is the photon flux at the photon energy E and $F(k,T,P)$ is a temperature- and position-dependent sampling function. Temperature scans were taken at the photon energies of 9.5, 10, 10.5, 11, 11.5, 12.3, 13.2, 14.35, 16.65 eV, to minimize the fragmentation influence. Additional signal corrections are applied to correct for ^{13}C and ^{18}O isomers, fragmentation and background signals. This analysis approach results in a reasonably good carbon balance of 100 ± 15%. PICSs of most intermediates are available in the literature [23]. For some highly reactive species such as HPMF which are expected to be key intermediates in the low-temperature oxidation processes of DME, cross sections were adopted from Ref. [11,24]. The resulting uncertainties of mole fractions for major species are typically within ±20%, while the uncertainties of the intermediate concentrations can range from 30% to a factor of 3, principally depending on the accuracy of the corresponding PICSs. As discussed in previous publications [11,21], the uncertainty on the temperatures was estimated to be within ±5%.

The mechanisms used in this work are a combination of an ozone sub-mechanism and different DME mechanisms. For kinetic modeling of the ozone decomposition, the O_3 sub-mechanism developed at Princeton University is employed [18], including the O_3 decomposition reaction and O_3 reactions with O, H, OH, HO_2, H_2O, CO, HCO, and CH_3. The direct reactions between O_3 and DME is supposed to be slow [12], and therefore the ozonolysis reactions of DME is of little importance and not considered in the mechanism. The kinetic of DME combustion has been investigated extensively, and several DME oxidation mechanisms [5,9,25-29] have been reported. Among the previous kinetic models, the widely used model which was proposed from the NUI Galway [27] was first chosen. The DME sub-mechanism in this model was comprehensively investigated in their previous kinetic studies [4,30,31], and validated against flow reactor, JSR data, rapid compression machine (RCM) and shock-tube ignition delay time, shock-tube speciation, laminar flame speed measurement and flame speciation. This model, coupled with O_3 sub-mechanism, is hereby referred to as "NUI model" hereafter. The second mechanism applied here is by Wang et al. [9]. The authors, based on the Zhao model [32], mainly updated reaction sequences that affect the low-temperature oxidation reactivity, such as the first O_2 addition to the fuel radical and isomerization of the methoxymethyl peroxy radical (RO_2). The model enabled an improved prediction of a wide range of experimental conditions, especially for the DME oxidation in the low-temperature regime. This model with the O_3 sub-

mechanism is named as "Wang model" herein. In this work, the simulations were carried out with the perfectly stirred reactor (PSR) module in the Chemkin Pro package [32]. Time-independent solutions were obtained using the transient solver with the end time set at 150 s.

3. Results and discussion

3.1 Influence of ozone addition on the detection of the species pool

Figure 1 presents the mass spectra from m/z=25 to 100 recorded under three different ozone addition levels at a photon energy of 11.2eV, taken at the temperature of 540 K. Many mass peaks were observed, corresponding to one or more combustion intermediates or fragment ions from photoionization. As can be seen from Fig.1, the mass spectra of the three cases are similar, indicating similar DME low-temperature reaction patterns despite the addition of ozone. To clarify the differences that result from ozone addition into the combustion system, we need to first interpret the complex mass spectra. In this work, the high mass resolution of the mass spectrometer (m/△m~4000) allows for the exact identification of the CH_2O_3 peak, that can be separated from contributions of ^{18}O isotopomers of $C_2H_4O_2$ isomers. Measurements of PIE spectra contain precise information of the ionization energies, which are crucial for species identification [34].

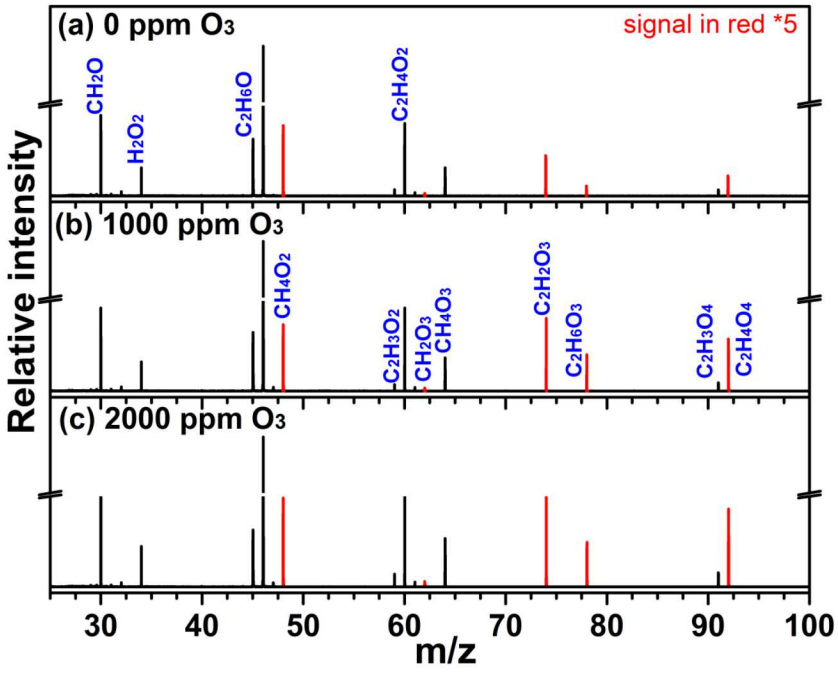

Fig. 1. Mass spectra recorded for three experimental cases (non-ozone, 1000 ppm O_3 and 2000 ppm O_3) at 540 K with the photoionization energy of 11.2eV. Some key intermediates related to the DME low-temperature oxidation are in red, whose relative ion signals are amplified with factors of 5.

A complete tabulation of these species is given in Table 2. It contains the values of photoionization energies, at which measurements were made, and PICSs taken from literatures, as well as the measurement uncertainty factors (*UF*s) for separate species. For a given mole fraction the *UF* is such that the uncertainty has a lower limit of x / *UF* and an upper limit of x × *UF*. In this work, a total of 25 species were detected and identified. In addition to those common low-temperature oxidation intermediates such as formaldehyde, hydrogen peroxide and formic acid, the identified species also include some peroxides (hydrogen peroxide, methyl peroxy, methyl hydroperoxide, methoxymethyl hydroperoxide (MMHP), HPMF). Other reactive molecules including 1,3-dioxirane, performic acid (PFA) and formic acid anhydride (FAA) were also observed. Overall, this work reproduces the results from our previous work [10,11] on the experimental confirmation of HPMF and other intermediates in the DME low-temperature oxidation. The detailed identification of some key species including HPMF, 1,3-dioxirane and MMHP, will be discussed below.

Table 2.

The list of detected intermediates in the low-temperature oxidation of DME. IE: ionization energy; E: photon energy used for quantification; PICS(E): photoionization cross section at the specific energy and references; UF: uncertainty factor of the peak mole fraction, which is defined such that for a measured mole fraction of *x*, the real value ranges from the lower limit of *x*/*UF* to the upper limit of *x*×*UF*.

m/z	Formula	Species	*IE*/eV	E/eV	*PICS*(E)		*UF*
					Mb	Ref.	
15.02	CH_3	Methyl	9.84	a	--	--	--
16.02	CH_4	Methane	12.61	13.2	4.72	[35]	1.5
18.01	H_2O	Water	12.62	--	--	--	1.2
26.01	C_2H_2	Acetylene	11.40	13.2	39.10	[36]	1.5
27.99	CO	Carbon monoxide	14.01	--	--	--	1.2

28.03	C_2H_4	Ethylene	10.51	11.5	8.02	[36]	1.5
30.01	CH_2O	Formaldehyde	10.88	11.5	13.17	[36]	1.5
30.05	C_2H_6	Ethane	11.52	13.2	15.90	[35]	1.5
31.99	O_2	Oxygen	12.07	--	--	--	1.2
32.03	CH_4O	Methanol	10.84	11.5	9.53	[36]	1.5
34.00	H_2O_2	Hydrogen peroxide	10.58	11.5	4.48	[37]	1.5
35.97	Ar	Argon	15.76	--	--	--	1.2
43.99	CO_2	Carbon dioxide	13.78	--	--	--	1.2
46.00	CH_2O_2	Formic acid	11.33	11.5	5.04	[36]	2.0
		1,3-Dioxirane	10.75	a	--	--	--
46.04	CH_3OCH_3	Dimethyl ether	10.03	--	--	--	1.2
47.01	CH_3O_2	Methyl peroxy	10.33	a	--	--	--
47.98	O_3	Ozone	12.53	--	--	--	1.2
48.02	CH_4O_2	Methyl hydroperoxide	9.83	10.5	2.42	[11]	3.0
60.02	$C_2H_4O_2$	Methyl formate	10.84	11.5	15.15	[38]	1.5
		1,3-Dioxetane	10.08	10.5	--	--	--
62.00	CH_2O_3	Performic acid	10.87	11.0	5.00	b	3.0
74.00	$C_2H_2O_3$	Formic acid anhydride	10.67	a	--	--	--
78.03	$C_2H_6O_3$	Methoxymethyl hydroperoxide	9.60	10.0	5.00	b	3.0
92.01	$C_2H_4O_4$	Hydroperoxymethyl formate	10.00	10.5	0.05	[11]	3.0

a: the quantification of this species cannot be achieved due to its bad signal/noise ratio;

b: estimated PICSs were used in the quantification

Ozone addition has a positive influence on the production of the highly reactive intermediates, as can be concluded from above speciation results. Increasing ozone addition results in remarkable increase of peak heights of these intermediates, as demonstrated by Fig. 1, where some key low-temperature intermediates are highlighted in red. Taking the signal of HPMF ($C_2H_4O_4$) as an example, a remarkable increase of signal-to-noise ratio could be achieved by the addition of ozone, bringing about nearly two times higher signal in the ozone case (2000 ppm) than that in the non-ozone case. A

possible explanation could be the enhanced reactivity of the system under the ozone condition. Specifically, the injection of O_3 seeds O into the combustion system, which could bring an exponential increase in the number of highly reactive radicals (typically OH). Compared with the non-ozone case, DME with O_3 addition demonstrates greater reactivity, along with higher production of low-temperature intermediates such as HPMF, and therefore the increase in the signal-to-noise ratio of some low-temperature intermediates can be achieved.

With the higher production of some intermediates in the ozone case, a higher detection efficiency of these intermediates was achieved. Subsequently, the smooth PIE curves of intermediates with visible thresholds could be easily gained, allowing for more unambiguous identification. The measured PIE spectra of some key intermediates at 540 K, are presented in Fig. 2. Figure 2a shows the PIE spectra of m/z =60.02, from which two thresholds can be observed. The higher one around 10.84 eV can be identified as the ionization energy of methyl formate, and the other is located around 10.08 eV, which matches the calculated ionization energy of 1,3-dioxetane [10]. The detection of methyl formate has been reported in several previous studies [6,7,9], while the observation of 1,3-dioxetane was only made in our previous work [10]. The JSR-sampled PIE curve for m/z = 92.01 ($C_2H_4O_4$) is shown in Fig. 2b. The agreement between the onset of the curve near 10.00 (±0.05) eV and the calculated IE of HPMF [10] can be obtained. Furthermore, the fragmentation reactions of HPMF can lead to different products including $HOOCH_2OC{\cdot}O$ (an H loss), $HOOCH_2OH$ (a CO loss) and $\cdot CH_2OCHO$ (an HOO-group loss). Their respective PIE curves can well match the calculated appearance energies (AEs) [10], as shown in Fig. 2b. HPMF, as the species responsible for degenerate branched chain reactions, plays a critical role in the low-temperature oxidation of DME [10]. However, very few studies describing the direct observation of HPMF are available. The existence of HPMF was recently proven in our previous work with the powerful diagnostic tool SVUV-PIMS. Besides these observations agreeing with the results from Ref. [10], some "new" species have been detected under ozone-seeded conditions. The JSR-sampled PIE curve for m/z = 78.03 ($C_2H_6O_3$) is shown in Fig. 2c. The measured threshold at 9.60 eV can be ascribed to the calculated ionization of MMHP [10], confirming the presence of this species. Another new detected intermediate was identified in mass spectra at m/z = 46.00 (CH_2O_2) for which the experimental PIE scan can be seen in Fig. 2d. The observed threshold near 10.75(±0.05) eV can be attributed to the photoionization of 1,3-dioxirane [10]. The formation of 1,3-dioxirane probably results from the isomerization of the Criegee intermediate $\cdot CH_2OO\cdot$[40]. The formation of the Criegee

intermediate was proposed as a favorable product of HPMF decomposition (an OH loss), and thus highlighted in DME combustion by Andersen et al. [41], but, to our knowledge, was not experimentally proven. The ·CH_2OO· radical is short-lived, and therefore its direct experimental detection is difficult. Recently, Rousso et al. [42] experimentally investigated relevant products of Criegee intermediate in the ozonolysis of ethylene system. Therefore, the new observation of MMHP and 1,3-dioxirane could be an evidence to support the effectiveness of the ozone-addition method in the detection of some highly reactive species.

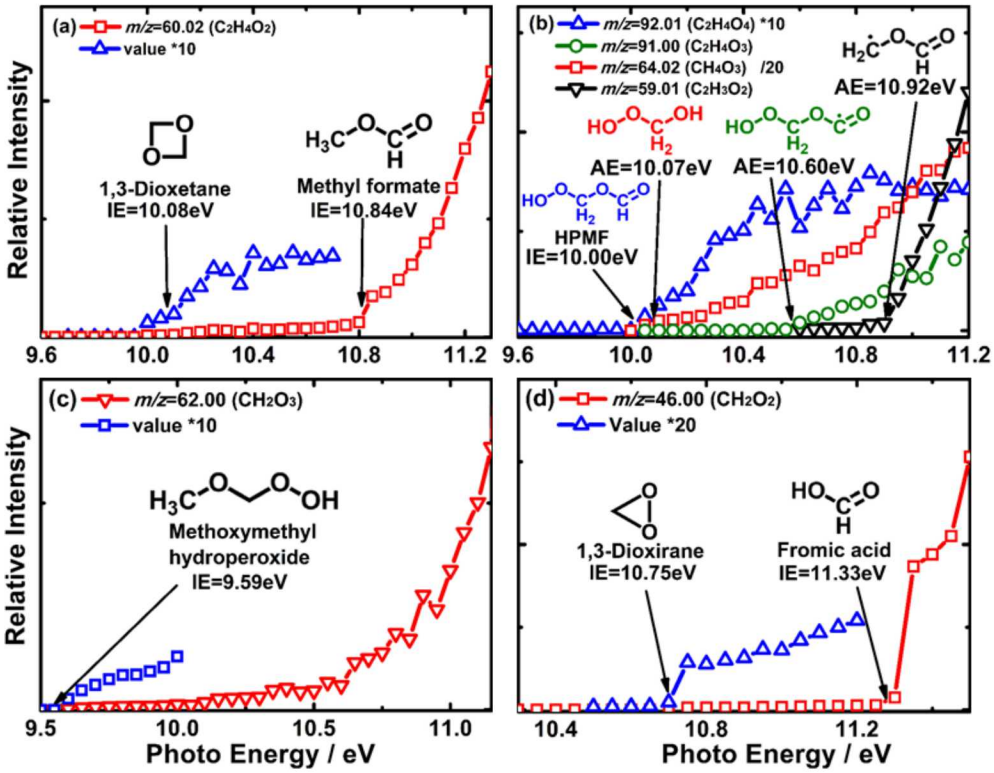

Fig. 2. Photoionization efficiency curves of (a) m/z = 60.02 ($C_2H_4O_2$), (b) m/z = 92.01($C_2H_4O_4$), (c) m/z = 62.00 (CH_2O_3) and (d) m/z = 46.00 (CH_2O_2) produced from the DME low-temperature oxidation with 2000 ppm O_3 addition at 500 K.

3.2 Influence of ozone addition on fuel consumption at low-temperature

Figure 3 depicts temperature-dependent mole fractions of major species (DME, O_2, O_3, H_2O, CO, CO_2) under three different ozone addition levels. The temperature measurement, from 400 to 800 K, covered the low- and intermediate-temperature regime. Clearly, the low-temperature oxidation threshold shifts towards lower temperatures, suggesting that the ozone addition could result in a significant rise in the reactivity. Taking the fuel DME as an example, little reactivity is observed until

the reactor temperature reaches 540 K in the ozone-free case (see Fig. 3a). For the ozone cases, the DME oxidation window is shifted to a lower temperature down to 480 K with 1000 ppm O_3 addition and 420K with 2000 ppm O_3 addition, as shown in the inset. Moreover, the enhancement of the reactivity of DME leads to increasing consumption of DME (30.0% for the non-ozone case, 41.3% for the 1000 ppm O_3 and 51.7% for the 2000 ppm O_3 at around 600 K). As temperature increases, the typical NTC behavior in which the reactivity decreases with temperature, still exists despite the addition of O_3. However, as the concentration of O_3 is increased, the NTC behavior tends to disappear, along with a much smaller fraction of fuel recovery over the NTC regime. The existence of the NTC zone is mainly due to the fact that the chain-branching process for the radical multiplication becomes less favored when temperature increases, and therefore the global reactivity of fuel goes down [43]. The presence of ozone would help to easily establish the radical pool, and consequently mitigate the loss of the fuel reactivity in the NTC region. Above 730 K, the fuel decreases monotonically with temperature, indicating the transition to the high-temperature kinetic regime. The onsets of the high-temperature reactivity are similar under different O_3 addition levels, suggesting that small addition of O atoms could hardly alter the high-temperature kinetics. For the formation of major species, DME consumption is accompanied closely by the rapid formation of H_2O, CO and CO_2, resulting in the formation of the first peak at the low-temperature regime (see Fig. 3d-f). As expected, the addition of O_3 reduces the formation temperature of these major species, displayed in the inset of Fig. 3d. In addition, with the increase of O_3 concentration, higher consumption of DME will lead to the higher peak concentrations of major species. Specifically, the higher O_3 addition (2000 ppm) yields a roughly 1.8-fold increase in the CO_2 conversion than that in the non-ozone case in the low-temperature regime.

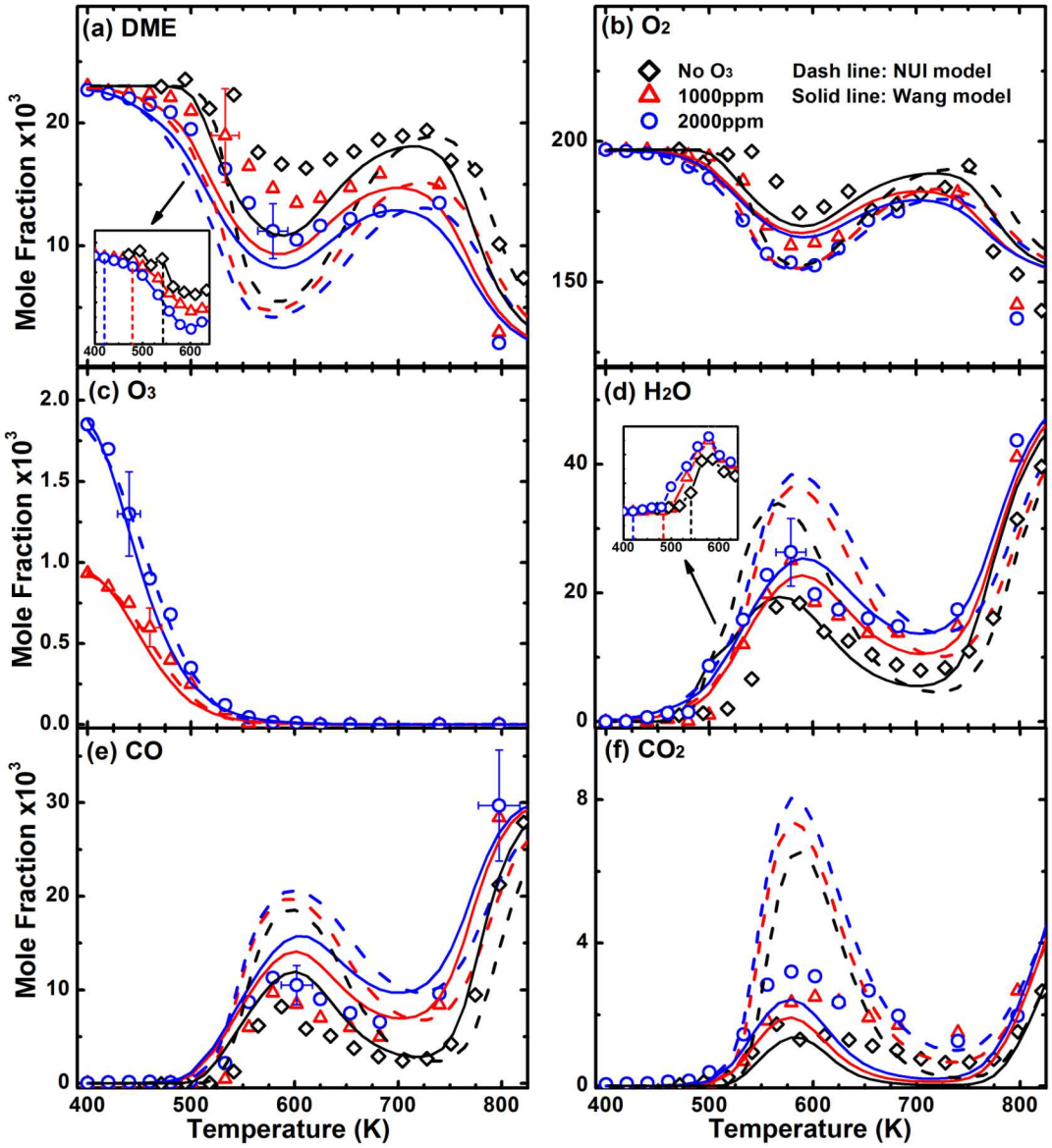

Fig. 3. Experimental mole fraction profiles and simulated results of the main species (DME, O_2, O_3, H_2O, CO, CO_2) as a function of temperature from 400 to 800 K under three different ozone addition levels. Symbols, measurements; dash lines, simulations with the NUI model; solid lines, simulations with the Wang model.

Comparisons between measured and modeled mole fraction profiles are also presented in Fig. 3. For the combustion kinetics investigation, predictions with the "NUI model" [27] and "Wang model" [9] (as described in Section 2) have been included. Both mechanisms reproduce the three distinct kinetic regimes, as observed in the experiments, well. However, there are some disagreements between simulated and experimental results. Although both models exhibit over-prediction for the fuel

consumption and corresponding formation of major species in the low-temperature regime, the Wang model shows a relatively better performance in general. Hence the following kinetic analyses were mainly based on the Wang model.

The schematic reaction network is established based on the rate of production (ROP) analysis, as depicted in Fig. 4. For all cases, the ROP analysis of the Wang model was performed at 510 K, at which the fuel began its low-temperature consumption for the ozone-free case. The presence of O_3 slightly complicates the chemical kinetics, but the fuel reaction patterns are almost the same despite the O_3 addition. Low-temperature oxidation of DME follows the classical sequence:

$$CH_3OCH_2 + O_2 = CH_3OCH_2O_2 \quad (R1)$$

$$CH_3OCH_2O_2 = CH_2OCH_2O_2H \quad (R2)$$

$$CH_2OCH_2O_2H + O_2 = O_2CH_2OCH_2O_2H \quad (R3)$$

$$O_2CH_2OCH_2O_2H = HOOCH_2OCHO + OH \quad (R4)$$

The HPMF ($HOOCH_2OCHO$), which is a degenerate branching agent, will subsequently decompose to give OH and the OCH2OCHO radicals. Besides the isomerization R2, the $CH_3OCH_2O_2$ radical would undergo other competing channels, i.e. its self-reaction:

$$2CH_3OCH_2O_2 = 2CH_3OCH_2O + O_2 \quad (R5)$$

$$2CH_3OCH_2O_2 = CH_3OCHO + CH_3OCH_2OH + O_2 \quad (R6)$$

The ROP results indicate that the H-atom abstraction by H atoms is favored with the increase of O_3 concentration. Figure 5 shows simulated concentration profiles of O and OH for various ozone addition levels. Clearly, ozone decomposition (at 400 K) generates a large amount of O atoms, which will mostly attack the fuel molecules to initiate the fuel oxidation. It is noted that O_3 acts mainly on the beginning of fuel oxidation, and the rest reaction network is mainly controlled by the chemistry of the fuel radical. In addition, the branching ratio of most competing reactions kept the same with and without O_3, except that of R2 and its competing pathways (R5+R6). The increase of the O_3 concentration weakens the predominant role of R2 and make R5 and R6 competitive at this temperature. It is well known that the role of QOOH through R2 is vital in the low-temperature oxidation of DME [9]. Especially, R2 will be highlighted at the early stage of low-temperature oxidation, by providing large amounts of OH radicals. As shown in Fig.5, the initial O atom originated from ozone decomposition strongly promotes the radical pool (typically OH). Subsequently, the significant increase in the concentration of OH will occur, which renders the DME low-temperature oxidation

become less dependent on R2, and then shifts the reaction path towards R5 and R6.

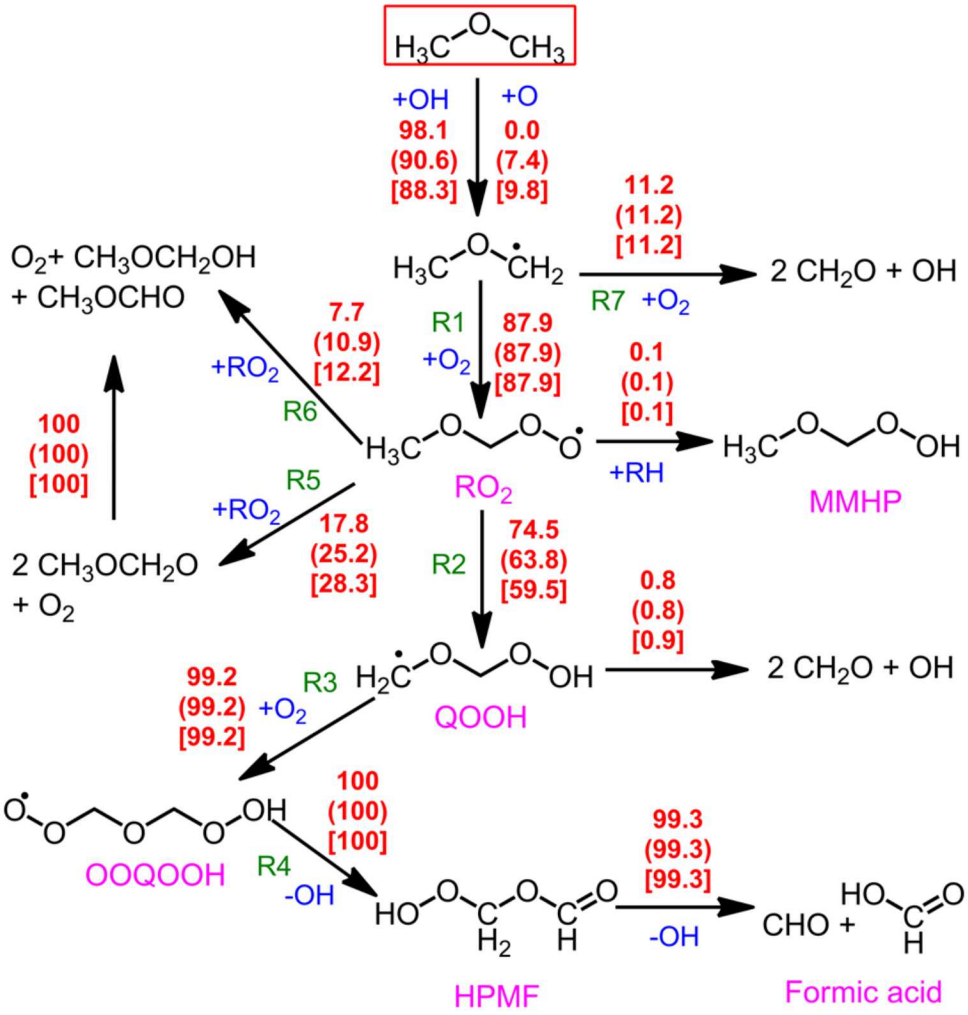

Fig. 4. Reaction pathways based on the ROP analysis for the DME low-temperature oxidation predicted by the Wang model. The ROP analysis was performed at 510 K. The numbers refer to the percent contribution to the consumption of the species on the source side with the O_3 addition of 0 ppm, 1000 ppm (in parentheses) and 2000 ppm [in square brackets].

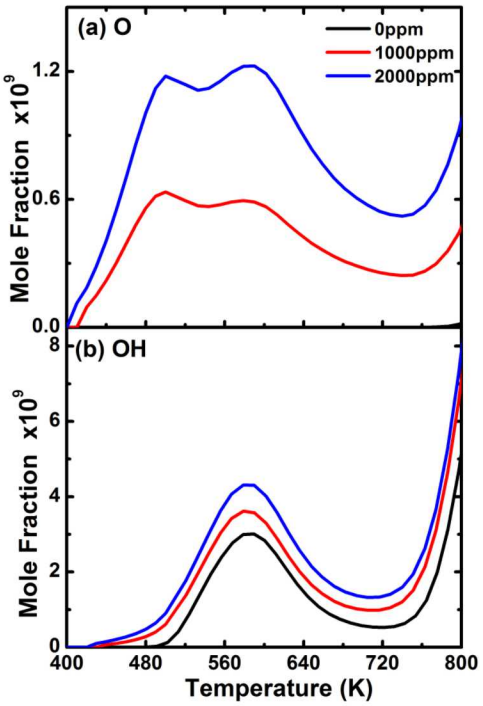

Fig. 5. Simulated mole fraction profiles of (a) the O radical and (b) the OH radical under three different ozone addition levels, using the Wang model.

Figure 5 also helps to understand the effects of ozone on the fuel consumption at different temperatures or ignition stages. At 500 K, the onset of the low-temperature reactivity, 2000 ppm ozone addition results in roughly 10-fold increase of OH radicals. While at 800 K, where the high-temperature kinetic oxidation occurs, 2000 ppm ozone addition only leads to approximately 1.5-fold increase of OH radicals. Therefore, it is not surprising that the effect of ozone is particularly pronounced at low temperature regime. In the case of high temperature combustion, the conventional oxidation pathways can lead to rapid oxidation, which explains the fact that ozone addition does not show much difference in the fuel high-temperature consumption (see Fig. 3). Special attention should be paid to the lower temperature regime for the ozone cases. Fig. 6 shows reaction flux of the fuel consumption at 400 K, 440 K and 480 K. In this temperature regime (especially $T < 440$ K), the fuel consumption prefers to proceed through R5 and R6 rather than the second oxygen addition pathway. Reaction $RO_2 \rightleftarrows$ QOOH equilibrium favors RO_2 within this very low temperature regime. This equilibrium is highly sensitive to temperature, and therefore the contribution of R2 increases as the temperature rises (see Fig. 6). At 400 K, the second oxygen addition pathways are nearly "frozen", and the ozone-assisted fuel consumption prefer to proceed through R5 and R6.

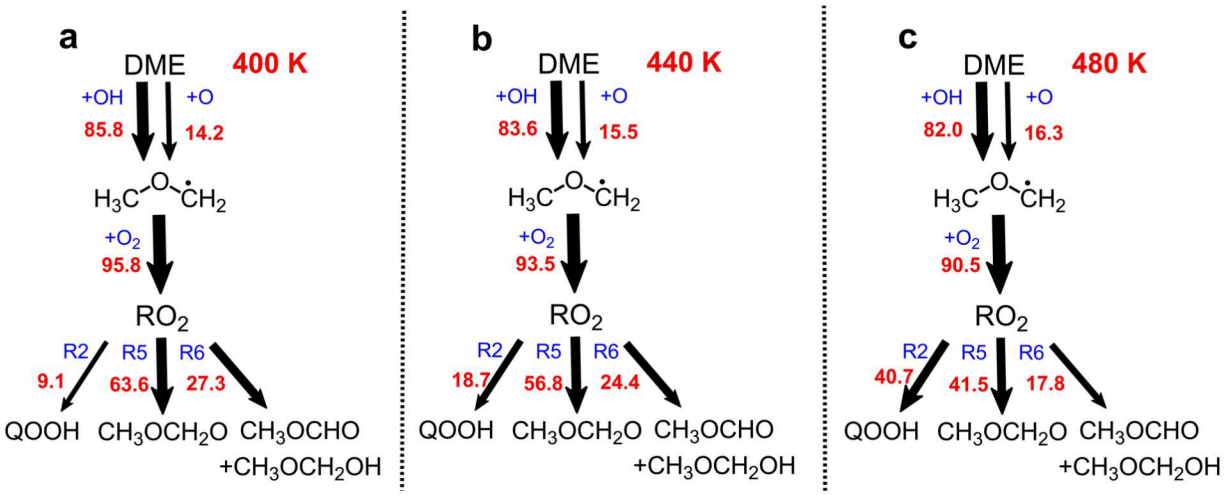

Fig. 6. Reaction flux of the fuel consumption through R1, R5 and R6, using the Wang model under (a) 400 K, (b) 440 K, and (c) 480 K for the 2000 ppm O_3 case. The thickness of each arrow denotes the reaction flux of corresponding pathway.

3.3 model development for ozone-assisted oxidation

Figure 7 depicts the measured mole fraction and model prediction of CH_2O and CH_3OCHO under different ozone addition levels. Considering that the ozone effects are more pronounced in the low-temperature regime, only the low-temperature data are presented here. More species mole fraction measurements are given in the Supplemental Material. CH_2O is a common intermediate in the low-temperature oxidation of hydrocarbons. As can be seen from Fig. 7a, an early production of CH_2O with ozone addition is observed as expected, showing significant production of CH_2O below 500 K. However, it is seen that both models under-predict the production of CH_2O within this low-temperature regime for all cases. Sensitivity analysis of CH_2O is carried out at 560 K for the ozone-free case, using the Wang model, as shown in Fig. 8a. It can be found that under such condition the formation of CH_2O is sensitive to several reactions, such as R1, R3, R6 and R7 ($CH_3OCH_2 + O_2 = 2CH_2O + OH$). Thanks to the ozone effect, the formation of CH_2O could be initiated at much lower temperatures, and we could conduct the sensitivity analysis of CH_2O at 460 K for the 2000 ppm O_3 case. As displayed in Fig. 8a, the number of reactions affecting the CH_2O formation significantly decrease. It is noteworthy that the sensitive reactions are only R1, R7 and the O_3-related reaction (R8: $O_3 + M \rightarrow O_2 + O + M$). The kinetics of the O_3-related reactions have been extensively investigated and considered to have a small uncertainty [12,44,45]. Also, as demonstrated in Fig. 1c, an excellent agreement can be seen between the measured and predicted distributions of O_3 under all tested conditions, indicating that the

uncertainty of O_3 decomposition rates contribute little to the overall uncertainty of the model prediction. Consequently, for the 2000 ppm O_3 case, the under-prediction of the CH_2O formation may be attributed to the overall contribution of R1 and R7, i.e., the over-estimated R1/R7 ratio. It is noted that a lower branching ratio R1/R7 was used in the Wang model than in the NUI model. In the Wang model, the branching ratios of R1 and R7 were taken from Rosado-Reyes et al. [46], in which the two product channels ratios were measured using the flash photolysis/transient infrared spectroscopy over the temperature range of 295-600 K. It might explain the better performance of the Wang model in predicting the DME low-temperature consumption and concentrations of CH_2O. Even so, an accurate determination of the branching ratios of R1 and R7 is worth exploring.

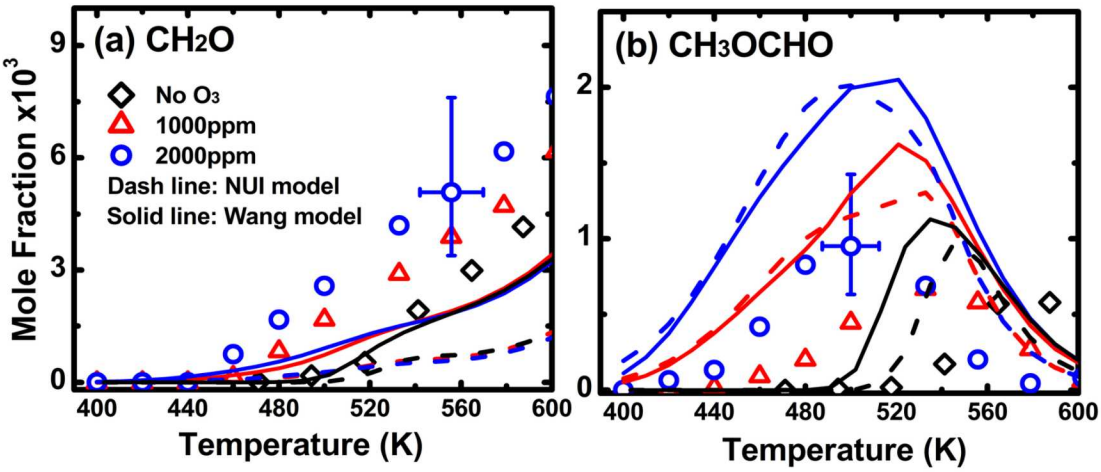

Fig. 7. Experimental mole fraction profiles and simulated results of (a) CH_2O and (b) CH_3OCHO as a function of temperature from 400 to 600 K under three different ozone addition levels. Symbols, measurements; dash lines, simulations with the NUI model; solid lines, simulations with the Wang model.

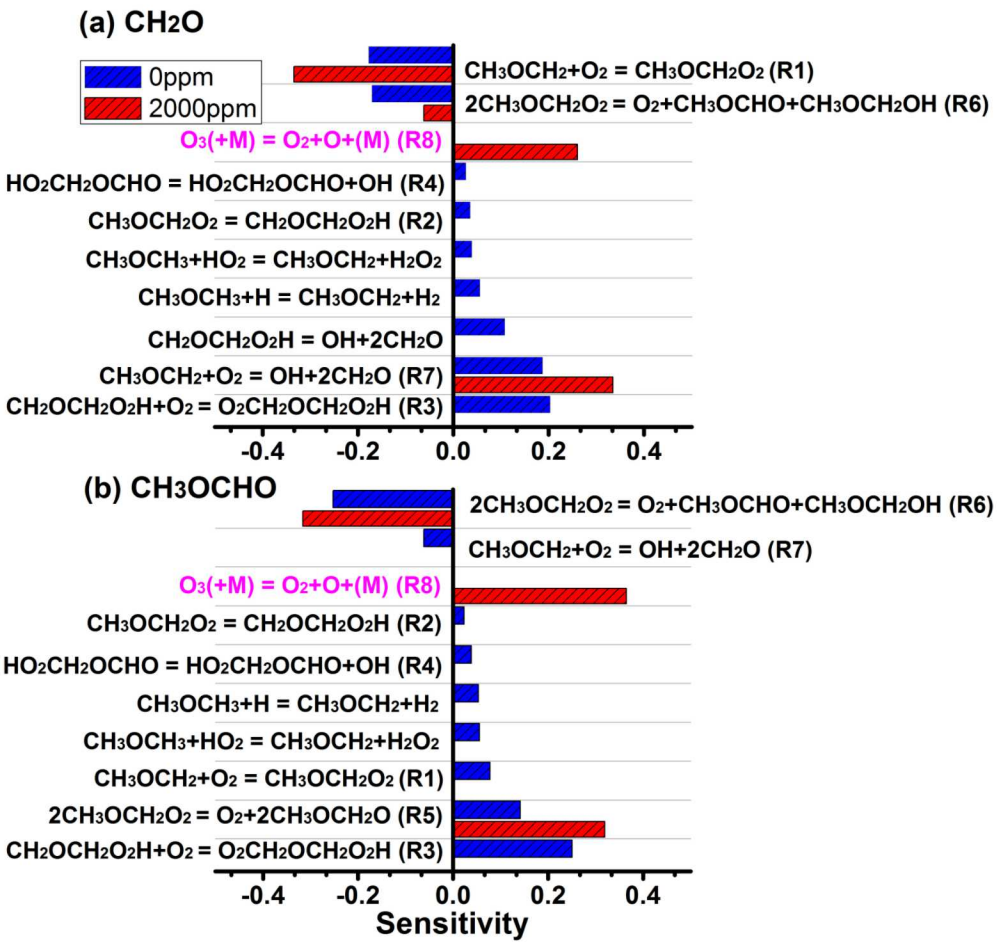

Fig. 8. Sensitivity analyses for (a) CH_2O and (b) CH_3OCHO concentrations in a JSR at 560 K (non-ozone) and at 460 K (2000 ppm O_3) using the Wang model. Only the ten most important reactions are listed.

CH_3OCHO is another important intermediate in the low-temperature oxidation of DME [6], whose mole fraction profiles are provided in Fig. 7b. The apparent broadening of the temperature window, affected by the ozone addition, is observed. The 1000 ppm and 2000 ppm ozone addition lowers the formation temperature window by ~60 K and ~120 K, respectively. However, for all cases, there is a discrepancy as both models over-predict the formation of CH_3OCHO. Sensitivity analyses of CH_3OCHO are also performed for the non-ozone case and the 2000 ppm O_3 case, as displayed in Fig. 8b. The results show that the CH_3OCHO formation is governed by the reactions of R5, R6 and R8 for the 2000 ppm O_3 case. The observed over-prediction of the CH_3OCHO formation may be due to the high branching ratio of R5/R6.

To obtain a deeper understanding of the influence of the ozone addition, sensitivity analyses work

were carried out. Fig. 9 shows the sensitivity analysis results of DME consumption, under the O_3 addition concentration from 0 ppm to 5000 ppm. It is found that with increasing the O_3 concentration, sensitivity coefficients of some reactions are getting smaller, whilst the O_3 decomposition (R8) tends to dominate the low-temperature oxidation of DME. Especially, the changes of reactions related to the second oxygen addition channel are obvious, such as R2 (isomerization of RO_2) and R4 (decomposition of OOQOOH). The sensitivity coefficients of these low-temperature-related reactions will reach their extremely low values under the condition of highest O_3 concentration. Moreover, the importance of R8 (in green) and R9 (the H-abstraction channel of fuel by OH, in dark gray) are highlighted under the condition of high O_3 concentration. A possible explanation might be that under the ozone cases, the injection of O_3 could lead to an exponential increase of reactive radicals into the system, and then the role of the low-temperature-related reactions for chain branching will be largely weakened. After the addition of O_3, the dominated reactions in the low-temperature oxidation of DME could be switched from a series of reactions to the combination of R8 and R9. Therefore, the ozone-doped experimental measurement could pass constraints to R8 and R9 causing the uncertainty of the model output. Given the small uncertainty of O_3-related reactions, the uncertainty of the kinetics of reaction R9 will become the primary uncertainty source. The concept proposed herein are expected to be useful for the experimental design for uncertainty minimization of combustion kinetic models. With the help of O_3 addition, some low-temperature-related pathways with relatively high uncertainties could be replaced by some O_3-related pathways with small uncertainties. As a consequence, the uncertainty of mole fraction distribution of a species could be dominated by a single reaction and some O_3-related reactions.

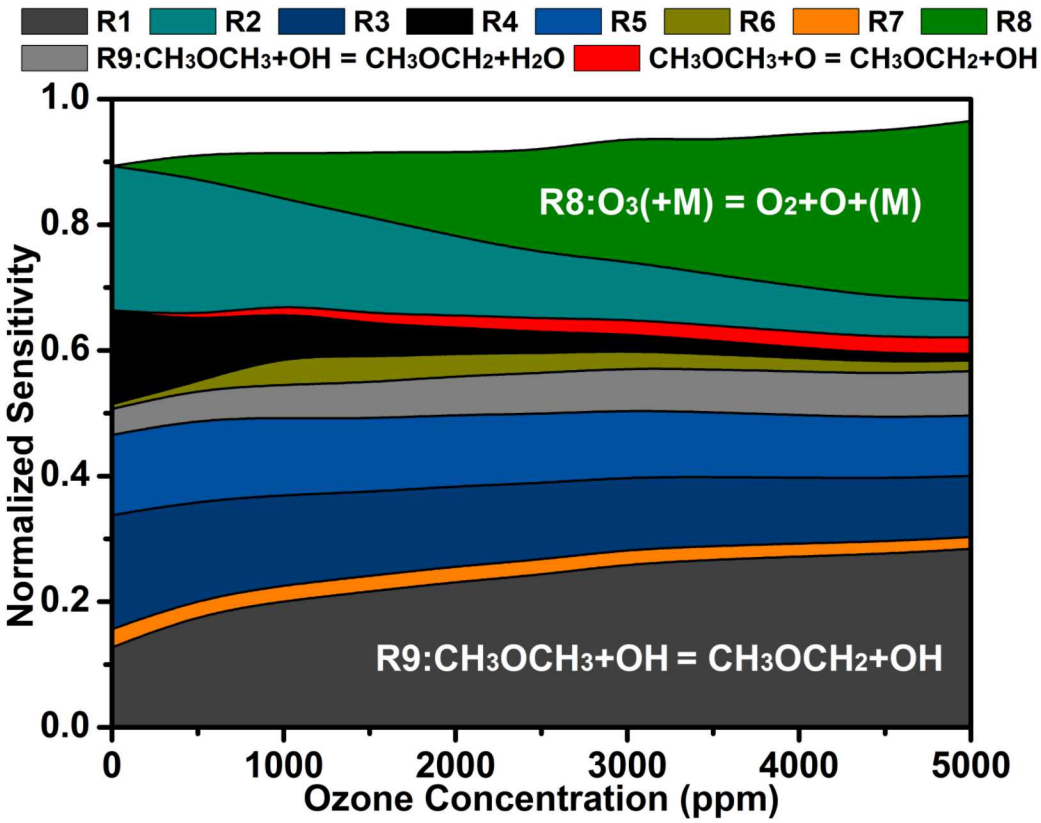

Fig. 9. Sensitivity coefficients of reactions, which control the DME low-temperature consumption, vary with the O_3 concentration from 0 ppm to 5000 ppm. Sensitivity analyses were carried out for DME concentrations in a JSR at 510 K using the Wang model.

4 Conclusions

The influence of ozone addition on the low-temperature oxidation of DME was experimentally investigated by employing a jet-stirred reactor coupled with the technique of SVUV-PIMS. Detailed species mole fraction variations with temperature from 400 to 800 K under O_3 addition of 1000 and 2000 ppm were obtained. The ozone addition demonstrates a positive influence on the production of the highly reactive intermediates. A total of 25 species were detected in this work, especially some elusive intermediates in the DME low-temperature oxidation such as methoxymethyl hydroperoxide, 1,3-dioxirane and hydroperoxymethyl formate.

Due to the ozone addition, the temperature window of fuel consumption and intermediates formation is shifted to much lower temperature regime. Hence, the ozone-addition method can help us to obtain the experimental results at lower temperature regime, where the traditional low-temperature oxidation cannot be initiated. These novel experimental data, together with modeling analysis, yield

some insights into fuel low-temperature oxidation. At low temperature regime (T < 440 K), temperature sensitive reactions such as the second oxygen channel are nearly "frozen", and the fuel consumption are dominated by recombination/disproportionation reactions of $CH_3OCH_2O_2$. Moreover, we also explored the intermediates (CH_2O and CH_3OCHO) formation in this special low-temperature regime (400 – 500 K), the results shown that the branching ratios of the $CH_3OCH_2O_2 + O_2$ reaction pathways and the $CH_3OCH_2O_2$ self-reactions need to be further modified.

Finally, we investigated the influences of the O_3 addition (0 – 5000 ppm) on the influential reactions, which controlled the fuel initial low-temperature oxidation. Our analysis shows that the number of influential reactions decreases, and some O_3-related pathways begin to show high sensitivity. These results suggested that some low-temperature-related pathways with relatively high uncertainties could be replaced by the ozone reactions with small uncertainties.

Acknowledgments

This work is supported by the National Natural Science Foundation of China (No. U1832192 and 51876199). The experiments profited from the expert technical assistance of Paul Fugazzi. This research used resources of the Advanced Light Source, supported by the Director, Office of Science, Office of Basic Energy Sciences, of the U.S. Department of Energy under Contract No. DEAC02-05CH11231. NH and KM were supported by the U.S. Department of Energy, Office of Science, Office of Basic Energy Sciences, Division of Chemical Sciences, Geosciences and Biosciences. Sandia National Laboratories is a multi-mission laboratory managed and operated by National Technology and Engineering Solutions of Sandia, LLC., a wholly owned subsidiary of Honeywell International, Inc., for the U.S. Department of Energy's National Nuclear Security Administration under contract DE-NA0003525.

References:

[1]C. Arcoumanis, C. Bae, R. Crookes, E. Kinoshita, The potential of di-methyl ether (DME) as an alternative fuel for compression-ignition engines: A review, Fuel 87 (2008) 1014-1030.

[2]T.A. Semelsberger, R.L. Borup, H.L. Greene, Dimethyl ether (DME) as an alternative fuel, J. Power Sources 156 (2006) 497-511.

[3]P. Dagaut, C. Daly, J.M. Simmie, M. Cathonnet, The oxidation and ignition of dimethylether from

low to high temperature (500 – 1600 K): Experiments and kinetic modeling, Proc. Combust. Inst 27 (1998) 361-369.

[4]H.J. Curran, S.L. Fishcer, F.L. Drye, The Reaction Kinetics of Dimethyl Ether. II: Low-Temperature Oxidation in Flow Reactors, Int. J. Chem. Kinet. 32 (2000) 741-759.

[5]Z. Zhao, A. Kazakov, F.L. Dryer, Measurements of dimethyl ether/air mixture burning velocities by using particle image velocimetry, Combust. Flame 139 (2004) 52-60.

[6]H. Guo, W. Sun, F.M. Haas, T. Farouk, F.L. Dryer, Y. Ju, Measurements of H2O2 in low temperature dimethyl ether oxidation, Proc. Combust. Inst 34 (2013) 573-581.

[7]F. Herrmann, B. Jochim, P. Oßwald, L. Cai, H. Pitsch, K. Kohse-Höinghaus, Experimental and numerical low-temperature oxidation study of ethanol and dimethyl ether, Combust. Flame 161 (2014) 384-397.

[8]N. Kurimoto, B. Brumfield, X. Yang, T. Wada, P. Diévart, G. Wysocki, Y. Ju, Quantitative measurements of HO_2 /H_2O_2 and intermediate species in low and intermediate temperature oxidation of dimethyl ether, Proc. Combust. Inst 35 (2015) 457-464.

[9]Z. Wang, X. Zhang, L. Xing, L. Zhang, F. Herrmann, K. Moshammer, F. Qi, K. Kohse-Höinghaus, Experimental and kinetic modeling study of the low- and intermediate-temperature oxidation of dimethyl ether, Combust. Flame 162 (2015) 1113-1125.

[10]K. Moshammer, A.W. Jasper, D.M. Popolan-Vaida, A. Lucassen, P. Diévart, H. Selim, A.J. Eskola, C.A. Taatjes, S.R. Leone, S.M. Sarathy, Y. Ju, P. Dagaut, K. Kohse-Höinghaus, N. Hansen, Detection and Identification of the Keto-Hydroperoxide ($HOOCH_2OCHO$) and Other Intermediates during Low-Temperature Oxidation of Dimethyl Ether, J. Phys. Chem. A 119 (2015) 7361-7374.

[11]K. Moshammer, A.W. Jasper, D.M. Popolan-Vaida, Z. Wang, V.S. Bhavani Shankar, L. Ruwe, C.A. Taatjes, P. Dagaut, N. Hansen, Quantification of the Keto-Hydroperoxide ($HOOCH_2OCHO$) and Other Elusive Intermediates during Low-Temperature Oxidation of Dimethyl Ether, J. Phys. Chem. A 120 (2016) 7890-7901.

[12]W. Sun, X. Gao, B. Wu, T. Ombrello, The effect of ozone addition on combustion: Kinetics and dynamics, Prog. Energ. Combust. 73 (2019) 1-25.

[13]Y. Zhang, K.P. Somers, M. Mehl, W.J. Pitz, R.F. Cracknell, H.J. Curran, Probing the antagonistic effect of toluene as a component in surrogate fuel models at low temperatures and high pressures. A case study of toluene/dimethyl ether mixtures, Proc. Combust. Inst 36 (2017) 413-421.

[14]H. Jin, J. Pieper, C. Hemken, E. Bräuer, L. Ruwe, K. Kohse-Höinghaus, Chemical interaction of dual-fuel mixtures in low-temperature oxidation, comparing n-pentane/dimethyl ether and n-pentane/ethanol, Combust. Flame 193 (2018) 36-53.

[15]C.B. Reuter, S.H. Won, Y. Ju, Experimental study of the dynamics and structure of self-sustaining premixed cool flames using a counterflow burner, Combust. Flame 166 (2016) 125-132.

[16]S.H. Won, B. Jiang, P. Diévart, C.H. Sohn, Y. Ju, Self-sustaining n -heptane cool diffusion flames activated by ozone, Proc. Combust. Inst 35 (2015) 881-888.

[17]C.B. Reuter, M. Lee, S.H. Won, Y. Ju, Study of the low-temperature reactivity of large n-alkanes through cool diffusion flame extinction, Combust. Flame 179 (2017) 23-32.

[18]H. Zhao, X. Yang, Y. Ju, Kinetic studies of ozone assisted low temperature oxidation of dimethyl ether in a flow reactor using molecular-beam mass spectrometry, Combust. Flame 173 (2016) 187-194.

[19]P. Dagaut, M. Cathonnet, J.P. Rouan, R. Foulatier, A. Quilgars, J.C. Boettner, F. Gaillard, H. James, A jet-stirred reactor for kinetic studies of homogeneous gas-phase reactions at pressures up to ten atmospheres (≈1 MPa), J. Phys. E: Sci. Instrum. 19 (1986) 207-209.

[20]W. Sun, T. Tao, M. Lailliau, N. Hansen, B. Yang, P. Dagaut, Exploration of the oxidation chemistry of dimethoxymethane: Jet-stirred reactor experiments and kinetic modeling, Combust. Flame 193 (2018) 491-501.

[21]T. Tao, W. Sun, N. Hansen, A.W. Jasper, K. Moshammer, B. Chen, Z. Wang, C. Huang, P. Dagaut, B. Yang, Exploring the negative temperature coefficient behavior of acetaldehyde based on detailed intermediate measurements in a jet-stirred reactor, Combust. Flame 192 (2018) 120-129.

[22]A.C. Rousso, N. Hansen, A.W. Jasper, Y. Ju, Low-Temperature Oxidation of Ethylene by Ozone in a Jet-Stirred Reactor, J. Phys. Chem. A 122 (2018) 8674-8685.

[23]Photonionization Cross Section Database (Version 2.0), National Synchrotron Radiation Laboratory, Hefei, China, 2017, http://flame.nsrl.ustc.edu.cn/en/database.htm .

[24]C. Huang, B. Yang, F. Zhang, Calculation of the absolute photoionization cross-sections for C1 – C4 Criegee intermediates and vinyl hydroperoxides, The Journal of Chemical Physics 150 (2019) 164305.

[25]D. Liu, J. Santner, C. Togbé, D. Felsmann, J. Koppmann, A. Lackner, X. Yang, X. Shen, Y. Ju, K. Kohse-Höinghaus, Flame structure and kinetic studies of carbon dioxide-diluted dimethyl ether

flames at reduced and elevated pressures, Combust. Flame 160 (2013) 2654-2668.

[26]A. Rodriguez, O. Frottier, O. Herbinet, R. Fournet, R. Bounaceur, C. Fittschen, F. Battin-Leclerc, Experimental and Modeling Investigation of the Low-Temperature Oxidation of Dimethyl Ether, J. Phys. Chem. A 119 (2015) 7905-7923.

[27]W.K. Metcalfe, S.M. Burke, S.S. Ahmed, H.J. Curran, A Hierarchical and Comparative Kinetic Modeling Study of C1 − C2 Hydrocarbon and Oxygenated Fuels, Int. J. Chem. Kinet. 45 (2013) 638-675.

[28]J.C. Prince & F.A. Williams, A short reaction mechanism for the combustion of dimethyl-ether, Combust. Flame 162 (2015) 3589-3595.

[29]E.E. Dames, A.S. Rosen, B.W. Weber, C.W. Gao, C. Sung, W.H. Green, A detailed combined experimental and theoretical study on dimethyl ether/propane blended oxidation, Combust. Flame 168 (2016) 310-330.

[30]U. Burke, K.P. Somers, P. O Toole, C.M. Zinner, N. Marquet, G. Bourque, E.L. Petersen, W.K. Metcalfe, Z. Serinyel, H.J. Curran, An ignition delay and kinetic modeling study of methane, dimethyl ether, and their mixtures at high pressures, Combust. Flame 162 (2015) 315-330.

[31]G. Mittal, S.M. Burke, V.A. Davies, B. Parajuli, W.K. Metcalfe, H.J. Curran, Autoignition of ethanol in a rapid compression machine, Combust. Flame 161 (2014) 1164-1171.

[32]Z. Zhao, M. Chaos, A. Kazakov, F.L. Dryer, Thermal Decomposition Reaction and a Comprehensive Kinetic Model of Dimethyl Ether, Int. J. Chem. Kinet. 40 (2010) 1-18.

[33]R. Kee, F. Rupley, J. Miller, M. Coltrin, J. Grcar, E. Meeks, H. Moffat, A. Lutz, G. Dixon-Lewis, M. Smooke, CHEMKIN-PRO Release 15082, Reaction Design, Inc., San Diego, CA, 2008.

[34]F. Qi, Combustion chemistry probed by synchrotron VUV photoionization mass spectrometry, Proc. Combust. Inst 34 (2013) 33-63.

[35]J. Wang, B. Yang, T.A. Cool, N. Hansen, T. Kasper, Near-threshold absolute photoionization cross-sections of some reaction intermediates in combustion, Int. J. Mass Spectrom. 269 (2008) 210-220.

[36]T.A. Cool, J. Wang, K. Nakajima, C.A. Taatjes, A. Mcllroy, Photoionization cross sections for reaction intermediates in hydrocarbon combustion, Int. J. Mass Spectrom. 247 (2005) 18-27.

[37]L.G. Dodson, L. Shen, J.D. Savee, N.C. Eddingsaas, O. Welz, C.A. Taatjes, D.L. Osborn, S.P. Sander, M. Okumura, VUV Photoionization Cross Sections of HO_2, H_2O_2, and H_2CO, J. Phys. Chem.

A 119 (2015) 1279-1291.

[38]J. Wang, B. Yang, T.A. Cool, N. Hansen, Absolute cross-sections for dissociative photoionization of some small esters, Int. J. Mass Spectrom. 292 (2010) 14-22.

[39]J. Gao & Y. Nakamura, Low-temperature ignition of dimethyl ether: transition from cool flame to hot flame promoted by decomposition of HPMF (HO_2CH_2OCHO), Combust. Flame 165 (2016) 68-82.

[40]R. Gutbrod, E. Kraka, R.N. Schindler, D. Cremer, Kinetic and Theoretical Investigation of the Gas-Phase Ozonolysis of Isoprene: Carbonyl Oxides as an Important Source for OH Radicals in the Atmosphere, J. Am. Chem. Soc. 119 (1997) 7330-7342.

[41]A. Andersen & E.A. Carter, Hybrid Density Functional Theory Predictions of Low-Temperature Dimethyl Ether Combustion Pathways. II. Chain-Branching Energetics and Possible Role of the Criegee Intermediate, J. Phys. Chem. A 107 (2003) 9463-9478.

[42]A.C. Rousso, N. Hansen, A.W. Jasper, Y. Ju, Identification of the Criegee intermediate reaction network in ethylene ozonolysis: impact on energy conversion strategies and atmospheric chemistry, Phys. Chem. Chem. Phys. 21 (2019) 7341-7357.

[43]H.J. Curran, Developing detailed chemical kinetic mechanisms for fuel combustion, Proc. Combust. Inst 37 (2019) 57-81.

[44]T. Ombrello, S.H. Won, Y. Ju, S. Williams, Flame propagation enhancement by plasma excitation of oxygen. Part I: Effects of O_3, Combust. Flame 157 (2010) 1906-1915.

[45]W.M. Jones & N. Davidson, The Thermal Decomposition of Ozone in a Shock Tube, J. Am. Chem. Soc. 84 (1962) 153-155.

[46]C.M. Rosado-Reyes, J.S. Francisco, J.J. Szente, M.M. Maricq, L. Frøsig Østergaard, Dimethyl Ether Oxidation at Elevated Temperatures (295−600 K), J. Phys. Chem. A 109 (2005) 10940-10953.